Supporting information

Thermoresponsive Magnetic Hydrogels as Theranostic Nanoconstructs

Manish K. Jaiswal[1,2], Mrinmoy De[2,3], Stanley S. Chou[2,3], Shaleen Vasavada[2], Reiner Bleher[2], Pottumarthi V. Prasad[4], D. Bahadur[1,5]*, V.P. Dravid[2,3]*

1. Metallurgical Engineering & Materials science
Indian Institute of Technology Bombay
Mumbai -40076, India.

2. Dept. of Materials Science & Engineering
Northwestern University
Evanston, IL-60208, USA

3. International Institute of Nanotechnology
Northwestern University
Evanston, IL 60208, USA

4. Department of Radiology
Evanston Northshore Healthcare
Evanston, IL 60201, USA

5. Centre for Research in Nanotechnology and Science
Indian Institute of Technology Bombay
Mumbai, MH 400076, India.

*Corresponding author:
Email address: v-dravid@northwestern.edu, dhirenb@iitb.ac.in

1. Synthesis of nitro-dopamine

The nitro-dopamine was obtained from dopamine hydrochloride following the method described in [1]. In brief, a solution of 5 g dopamine hydrochloride and 6.3 g sodium nitrite in 150 mL water chilled in an ice bath was added with 25 mL of 20% HCl drop-wise. The solution turned into yellow solid due to the formation of nitro-dopamine hydrogensulphate which was then separated and collected by filtration. The obtained nitro-dopamine hydrogensulphate was added under stirring to a solution of $SnCl_2.2H_2O$ in conc. HCl and the resulting mixture was maintained at 80 °C for ½ h. After cooling, the solid separated, filtered and collected.

2. X-ray diffraction and FT-IR spectra

Figure S1 (a, b) shows the X-ray diffraction pattern and Fourier-transform infra-red (FT-IR) spectra of the oleic acid coated Fe_3O_4 magnetic nanostructures (MNS) respectively. The X-ray peaks recorded for MNS of the sizes 9 and 12 nm in the range of 25 to 70° using CuK_{α}, λ=1.5405 Å radiation are indexed in figure (a). The presence of all major characteristic peaks confirms the formation of magnetite phase in the synthesized MNS samples[2].

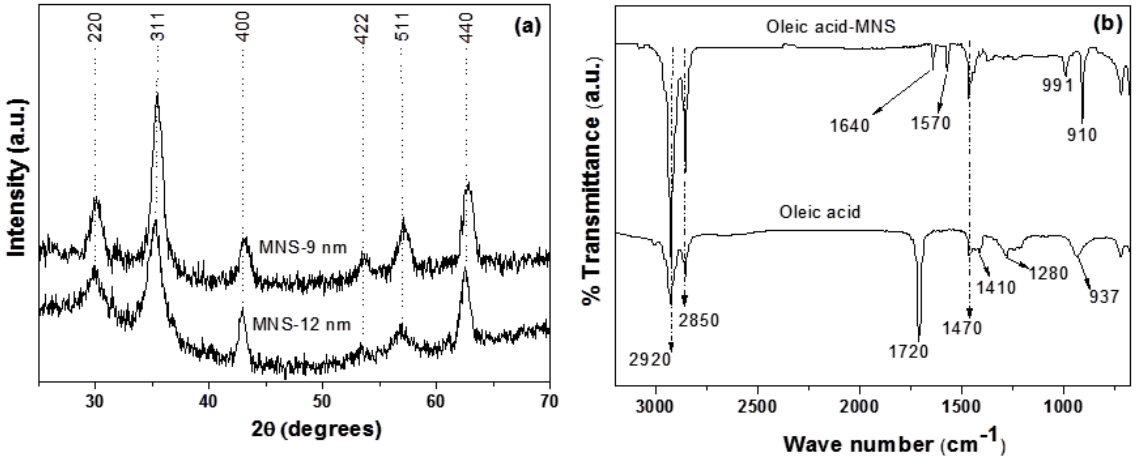

Figure S1: (a) X-ray diffraction pattern and (b) Fourier-transform infra-red spectra of oleic acid Fe_3O_4 MNS.

FT-IR spectra shown in figure (b) confirm the coating of oleic acid onto Fe_3O_4 MNS via bidentate covalent bonding of COO^- to the Fe atoms on the MNS surface. The band appeared at 1720 cm^{-1} assigned to >C=O of carboxylate group in the neat oleic acid has disappeared after binding with MNS. Two new peaks instead at 1640 and 1570 cm^{-1} have appeared in the spectra of MNS coated with oleic acid which indicated the symmetric (ν_s) and anti-symmetric (ν_{as}) stretching of COO^- respectively. Their difference (Δ = 90 cm^{-1}) of ν_s and ν_{as} corresponds to the chelating bidentate type of covalent binding[3]. Further the vibrational bands at 2920 and 2850 cm^{-1} are due to the symmetric and asymmetric stretching mode of CH_2. The peak at 3010 cm^{-1} can be assigned to ν (=CH-) stretching mode in trans-configuration.

3. X-ray photo electron spectra (XPS)

To confirm the ligand exchange of oleic acid by PEG-diacid and POSS we carried out X-ray photoelectron spectra (XPS) analysis of the functionalized-Fe_3O_4 MNS. Figure S2 shows the binding energy vs. intensity spectra for Fe core $2p_{3/2}$ and $2p_{1/2}$ levels of Fe_3O_4-MNS coated with hydrophobic oleic acid and hydrophilic POSS and PEG-diacid ligands. The Fe binding energy peaks corresponding to oleic acid appeared at 709.7 and 723.5 eV for $2p_{3/2}$ and $2p_{1/2}$ states respectively[4]. These peaks are observed shifted to lower values of 709.1 and 722.5 eV when replaced by PEG-diacid and to 709.0 and 722.6 eV when replaced by POSS respectively onto the MNS surface. The lowering in binding energies after ligand replacement can be attributed to the enhanced de-shielding of Fe atoms when attached either with PEG or POSS molecules. As shown in the schematic in figure 2, the oxygen atoms of oleic acid bound to Fe atoms of MNS are replaced by oxygen atoms of PEG and POSS molecules after ligand exchange which provide it more de-shielding and hence enhance the kinetic energies of $2p_{3/2}$ and $2p_{1/2}$ states and reduces the associated binding energy.

Figure S2 (b) shows the O 1*s* peak for oleic and PEG-diacid coated Fe_3O_4-MNS. As can be seen from the figure the peak appeared at 528.7 is shifted to 529.3 eV when oleic acid is replaced by PEG-diacid onto the surface of MNS. As shown in the figure 2, the oxygen atom from oleic acid bind with Fe atom is replaced by two oxygen atoms from PEG-diacid. Simultaneously co-ordination of two oxygen atoms of PEG-diacid, which has more bulkier groups causing less kinetic energy. Therefore, there is an upward shifting in binding energy. Further the shoulder detected at 530.8 eV accompanied by the main peak can be ascribed to the absorbed H_2O in the form of moisture due to the increased hydrophilicity of the nanostructure surfaces after PEG coating[5]. On similar lines POSS O 1s peak is found to be shifted to 530.7 eV which can be attributed to the replacement of oleic acid by cage-shaped silica groups offering higher aqueous stability.

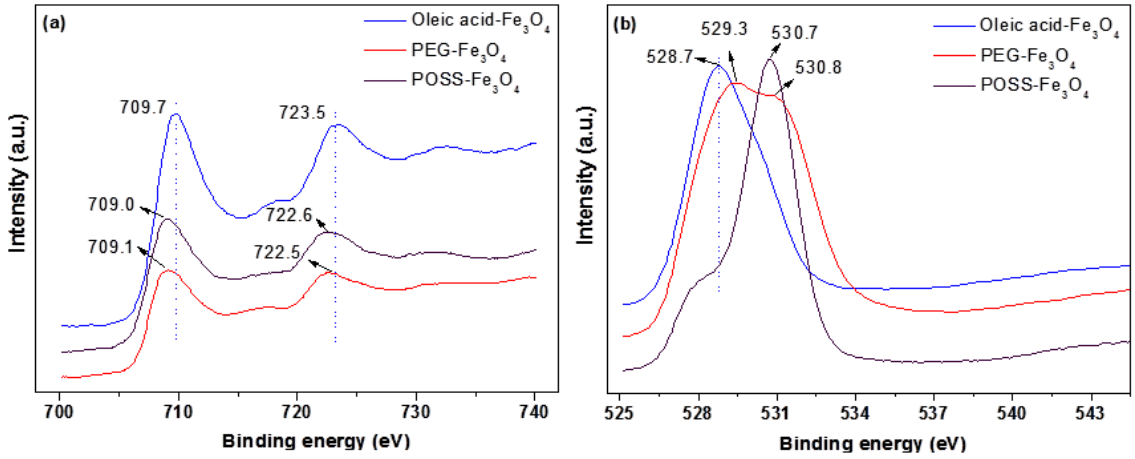

Figure S2: X-ray photoelectron spectra for (a) Fe 2*p* core-level (b) O 1*s* core-level of Fe_3O_4 MNS coated with PEG-diacid and POSS along with that of hydrophobic oleic acid.

4. Nuclear magnetic resonance (NMR) spectra

Free radical polymerization reaction of NIPAAm was carried out to synthesize its polymeric hydrogels. To confirm the polymerization, ^{13}C cross polarization-magic angle spinning (CP-MAS) solid state NMR spectra of both monomer and polymer were recorded

using Varian-400 machine operating at 400 MHz. The sample probe was 5 mm HXY sealed with Kel-F cap, spinning at 8 kHz about applied magnetic field under ambient conditions. The figure S3 shows the NMR spectra for chemical shifts in carbon nuclides for monomer along with its polymer counterpart.

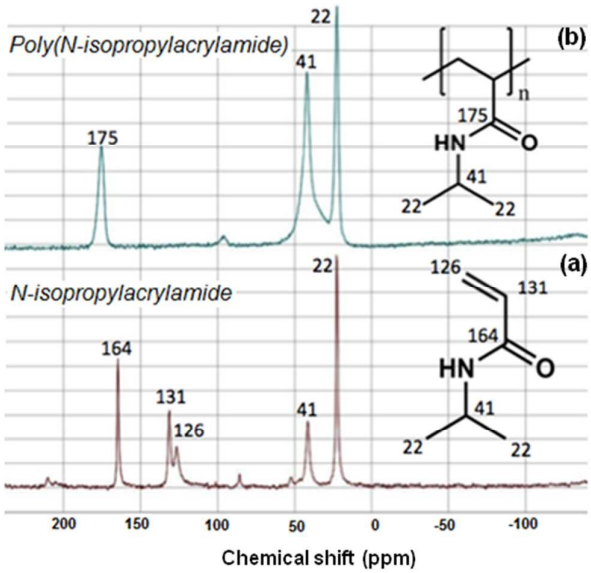

Figure S3: Solid state ^{13}C NMR spectra of (a) NIPAAm and (b) poly(NIPAAm) confirming the polymerization.

As shown in the figure S3 (a, b) the chemical shifts obtained at δ 22 and δ 41 ppm which can be assigned to methyl and isopropyl methine groups respectively remained unaltered after polymerization. Further the signals corresponding to vinyl carbon nuclei detected at δ 126 and δ 131 ppm in the figure S3 (a) have disappeared in the figure S3 (b) due to up-field shift after polymerization. As can be seen from figure S3 (b) the signal obtained at δ 41 ppm appears broader due to the merger of isopropyl methine carbon peak and shifted signals originated from breaking of double-bond of vinyl group as well which facilitates the formation of a long chain polymer. In addition the signal corresponding to the carbonyl group at δ 164 ppm in monomer (figure S3 a) has little shifted to downfield at δ 175 ppm (figure S3

b) which can be attributed to the enhanced de-shielding effect in its proximity after long chain formation.

5. Iron concentration & magnetization measurement

The iron estimation in all samples was carried out through ICP-AES (inductively coupled plasma-atomic emission spectroscopy) technique, using Varian-vista model. For PEG and POSS functionalized MNS 50 µL of aqueous suspended fluid was digested into 250 µL conc. HNO_3 and total volume was made up to 5 mL with water. For hydrogels-MNS, 5 mg sample was first dispersed into 1 mL water and 50 µL of it was digested into 250 µL conc. HNO_3 which was further made up to 5 mL with water.

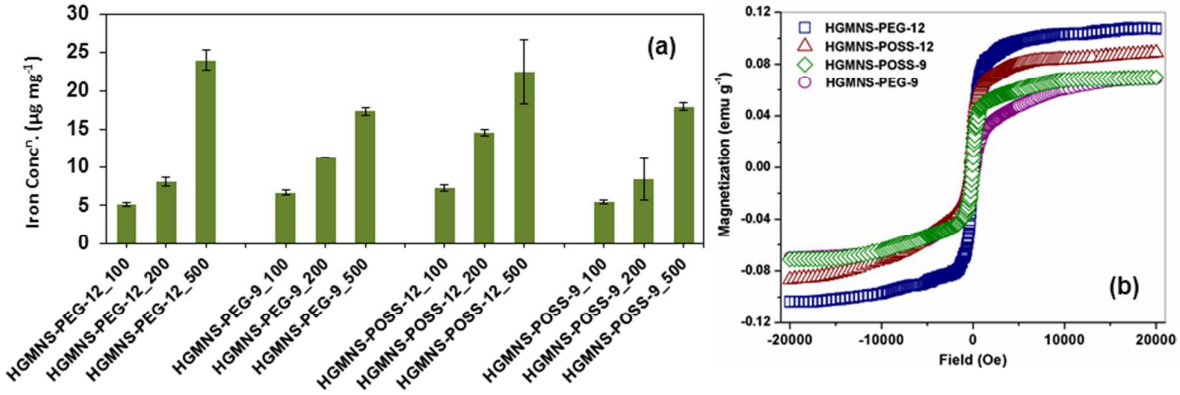

Figure S4: (a) Iron concentration into hydrogel-MNS sample measurement through ICP-AES technique expressed in microgram per milligram of the sample. Data are expressed as mean ± s.d. (n=3). {Notation HGMNS-PEG-12_100 indicates hydrogel sample synthesized in presence of 100 µg iron of 12 nm PEG-Fe_3O_4}. (b) Magnetization values of the HGMNS samples with highest iron content for both the sizes (9 and 12 nm) of Fe_3O_4 MNS.

Figure S4 (a) shows the iron concentration into the hydrogel-MNS samples and S4 (b) magnetization measurements of samples with highest iron contents; HGMNS-PEG-12, HGMNS-POSS-12, HGMNS-PEG-9, and HGMNS-POSS-9. For sample preparation, 5 mg mL^{-1} aqueous solution of each sample was prepared out of which 50 µL was digested into

250 μL HNO_3 in triplicates which was further made to 5 mL by adding water. The highest iron concentration values obtained for HGMNS-PEG-12, HGMNS-POSS-12, HGMNS-PEG-9, and HGMNS-POSS-9 are; approximately 24, 22, 27, and 18 μg mg^{-1} for MNS feed amounts of 500 μg of iron in NIPAAm precursor. Also as indicated by the data hydrogels with 12 nm has more iron content than 9 nm MNS size for both PEG and POSS functionalized Fe_3O_4 based MNS which is consistent with the fact that bigger the size more is the iron content.

Magnetization measurements carried out through SQUID magnetometer (superconducting quantum interference device, Quantum design, MPMS, USA) showed that that the hydrogels with larger size of MNS (12 nm) exhibit higher value of magnetic moment than their smaller size (9 nm) counterpart. Overall the highest magnetization is obtained for HGMS-PEG-12 which is approximately 0.11 emu g^{-1} at the field of 20,000 Oe, slightly higher than HGMNS-POSS-12 (0.09 emu g^{-1}) which indicates higher coating thickness of POSS onto MNS surface. Further the practical measured value of magnetization for HGMNS-12 via SQUID appears to be lesser than that if calculated using ICP-AES data for the iron concentration. In order to understand the difference we carried out thermo-gravimetric analysis (TGA) of the sample. Figure S5 shows the TGA plot of HGMNS-12 along with HG which is used as a reference material to calculate the residual MNS after polymeric decomposition obtained up to 450 °C. As shown in the figure S5 (b) the difference in weight % in HGMNS-PEG-12 and HG is approx. 1.5% which accounts for Fe_3O_4 MNS. A rough calculation gives the value of magnetization to be roughly less than 1 emu g^{-1} which is consistent with that of obtained from ICP-AES. So we believe the difference is possibly due to the experimental error range at low magnetization measurement.

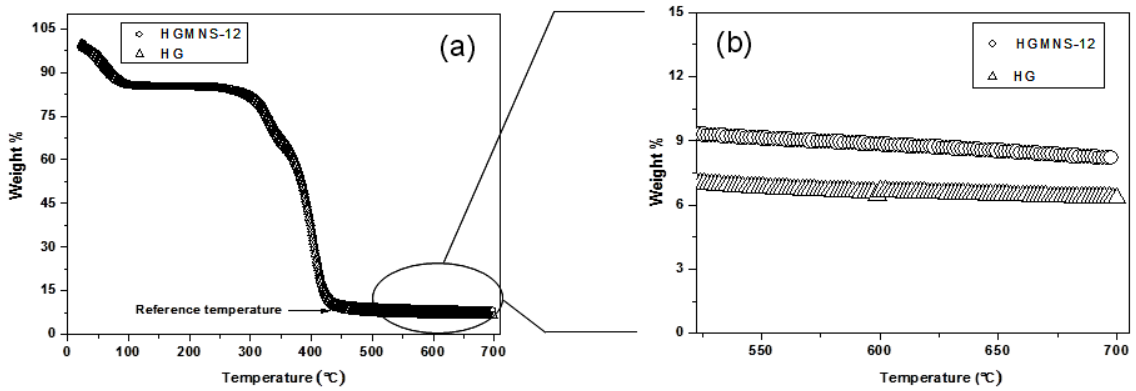

Figure S5: (a) Thermo-gravimetric analysis (TGA) of the samples HGMNS-PEG-12 along with hydrogel (HG). (b) The magnified picture of selected section of data presented in (a).

6. Drug encapsulation and release protocol of hydrogel-MNS samples

As discussed in the section 2.3 of the manuscript the release efficacy of hydrogels were studied under water-bath (set at 42 ± 2 °C) and RF field assisted (5 kW, 230 kHz, 180 Oe) system and compared with that of room-temperature (No RF). For encapsulation, 4 mg of sample and 100 (or 50) µg DOX (or fluorescein) were properly dispersed/sonicated in 500 µL water in micro-centrifuge tubes in triplicates kept for overnight at 4 °C. The thus obtained sample loaded with cargo was centrifuged at 12,000 rpm at 4 °C for 10 min to separate out the unloaded drug. The surface bound fluorophore was removed by washing with 500 µL chilled water and centrifuging to separate out the supernatant thrice. All the supernatant were collected and further subjected to micro-plate reader to estimate the unloaded amount of drug which ultimately yielded the loaded amount of drug into the hydrogel samples. For the release of fluorophore, sample loaded with drug was homogenously mixed in 3 mL water and trifurcated into three different micro-centrifuge tubes with 1 mL in each. The three tubes were further subjected with water-bath (tube 1, 42 ± 2 °C), RF (tube 2, 5 kW, 230 kHz, 180 Oe) and control (tube 3, no RF exposure) at room temperature for 1 h simultaneously. Subsequently all the tubes were centrifuged at 10,000 rpm for 10 min and supernatant which contains released drug was collected for estimation using micro-plate reader. The emission

spectra of fluorescein and DOX shown in figure S6 were obtained by exciton wavelength of 490 nm. The loading of cargos in hydrogels are calculated by difference in intensity unit numbers of total (control) and unloaded part.

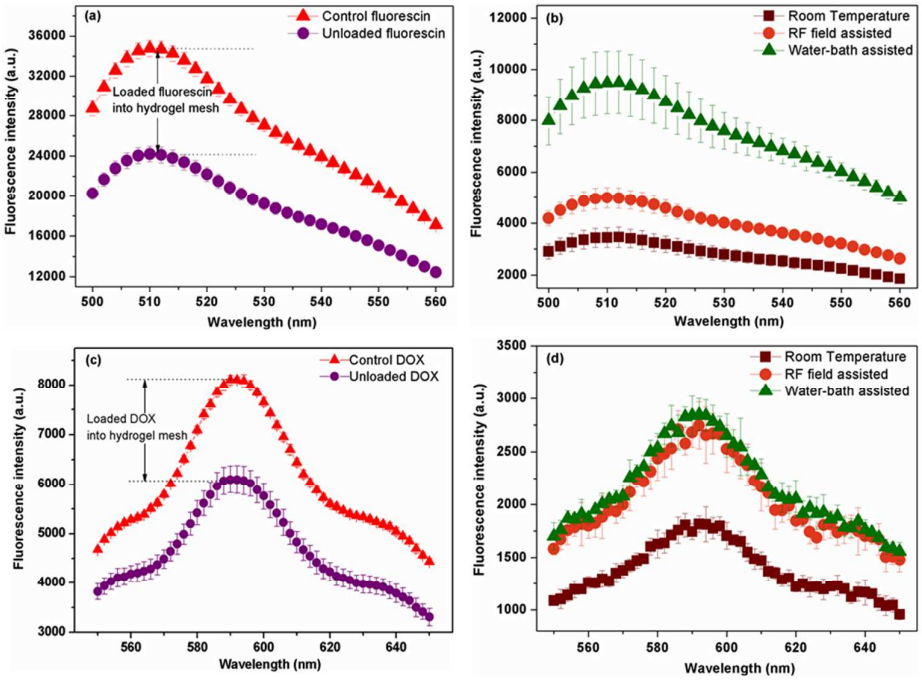

Figure S6: Representative fluorescence evolution spectra of (a, b) fluorescein and (c, d) DOX encapsulation and release. The difference of control and unloaded part yields to the estimation of loaded cargo into hydrogel as represented by (a) and (c).

As mentioned in the results and discussion section of the manuscript the values of encapsulation efficiency (EE), feed weight ratio (FWR) and loading content (LC) for DOX were calculated to be approx. 25 % or 6 µg mg^{-1} or $3.6x10^{-11}$ µg/hydrogel (EE), 2.5 % (FWR) and 0.625 % (LC) while for fluorescein these values were 30 % or 3.75 µg mg^{-1} or $2.2x10^{-11}$ µg/hydrogel (EE), 1.25 % (FWR) and 0.375 % (LC) respectively.

Figure S6 shows the representative release behavior of (b) fluorescein from HGMNS-9 and (d) DOX from HGMNS-12 from studied under different conditions. The release of DOX from the sample under water-bath, RF field assisted and No RF (room temperature)

conditions were obtained approx. 3.57, 3.45 and 2.25 μg mg^{-1} respectively. It is instructive to note that the temperature of the liquid containing the hydrogel during application of RF field for 1 h was monitored and it remained unchanged macroscopically throughout the experiment. However, the fluorescence spectral intensity for RF field induced DOX released is close to that of released under water-bath assisted system which can be attributed to effect of localized heat as well magnetic oscillations. It is noteworthy that similar experiments carried out using 9 nm MNS, HGMNS-PEG-9 yielded into 2.3 μg mg^{-1} DOX release under RF field assisted delivery which can be attributed to the low heat generation due to smaller size MNS. For fluorescein the release amounts were 0.67 and 1.3 μg mg^{-1} under RF field for HGMNS-PEG-9 and HGMNS-PEG-12 samples respectively.

7. Cumulative DOX release

The cumulative DOX release from the sample HGMNS-PEG-12 was studies under water-bath set-up at temperatures 37 and 44 °C to mimic physiological and cancer therapeutic temperatures respectively.

In a typical experiment 4 mg samples in two batches loaded with approx. 30 μg DOX in each were taken into 1 mL PBS (0.1 M, pH 7.4) in dialysis bags (Mol. wt. cut-off ~ 10,000 Da). The bags were then submerged in 250 mL release media of PBS in two separate beakers maintained at 37 and 44 °C respectively. The PBS in the beakers was made to stir continuously with a magnetic stirrer. The entire set-up was covered with aluminum foil to avoid any kind of photo-bleaching. 1 mL of the aliquot was drawn from the release media at different predetermined time points and substituted with equal amount of fresh PBS to maintain the sink conditions. The collected released DOX were then plated in 96-well plate and the cumulative released amounts in 1800 min were estimated using DOX standard calibration curve shown in figure S7 (b).

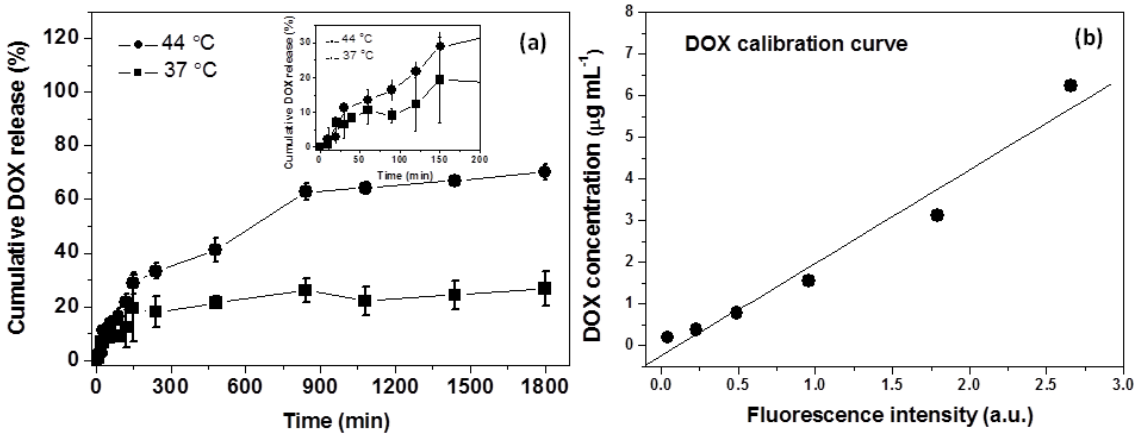

Figure S7: (a) Cumulative drug release profile from the sample HGMNS-PEG-12 at two different temperatures, 37 and 44 ° C for doxorubicin (DOX). Inset in the figure is the magnified plot of released DOX in the first 200 min from the sample. (b) Shows the standard calibration curve for DOX.

Figure S7 (a) shows the observed cumulative DOX release up to 1800 min for both 37 and 44 °C. As can be seen from the plot the total release of DOX were approx. 70.2 ± 3 and 26.8 ± 6.4 % at 44 and 37 °C respectively which demonstrates the thermo-responsive nature of the material. Also the obtained profiles indicate after the initial burst release of DOX, shown in the magnified inset images in fig. S7 (a), it attained a sustain behavior of release which is necessary to treat and further prevent the proliferation of cancer cells.

8. STEM imaging of hydrogels at elevated temperatures

As can be seen from the figure S8 (a, b) the hydrogel morphology appears disrupted and aggregated after cell uptake due to the processing temperature of STEM sample preparation. To confirm that aggregation was not caused by the cell environment, we carried out STEM imaging of hydrogel samples that were exposed to elevated temperatures; 30, 40, 50 and 70 °C respectively. It was observed that no morphological change/distortions occurred with heating up to 50 ºC, however at 70 ºC the hydrogels appeared quite fused together while

losing their spherical identity. The images shown in figure S8 (c, d) indicate that the disruption of hydrogel structure, that was observed in section of cells occurred during polymerization of embedding resin at 60 ºC.

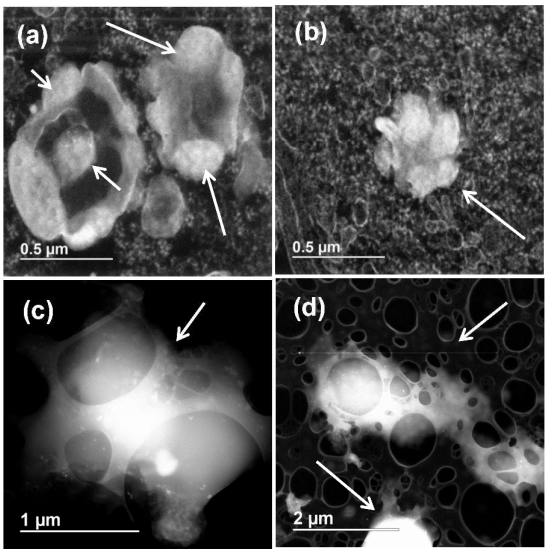

Figure S8: STEM images of (a, b) cell uptake of hydrogels along with (c, d) the sample after being exposed to 70 °C for 24 h. (The darker circles in the background of (c) and (d) are due to lacey carbon grids.)

References

1. Iapolitano, A.; Irrchia, M.; Costantini, C.; Prota, G. *Tetrahedron* **1992**, 48, 8515-8522.

2. Jaiswal, M. K.; Mehta, S.; Banerjee, R.; Bahadur, D. *Colloid. Polym. Sci*. **2012**, 290, 607-617.

3. Zhang, L.; He, R.; Gu, H.-C. *Appl. Surf. Sci.* **2006**, 253, 2611–2617.

4. Preisinger, M.; Krispin, M.; Rudolf, T.; Horn, S.; Strongin, D. R.; *Phys. Rev.* B **2005**, 71, 165409.

5. Prakash, A.; Chandra S.; Bahadur, D.; *Carbon* **2012**, 50, 4209-4219.